On the Fill Charge and the Sensitivity Analysis of a V-Shaped Micro Heat Pipe

Balram Suman
Dept. of Chemical Engineering and Materials Science, University of Minnesota, Minneapolis, MN 55455

DOI 10.1002/aic.10941
Published online July 17, 2006 in Wiley InterScience (www.interscience.wiley.com).

The fill charge and the sensitivity analysis of a micro-grooved heat pipe are presented. Methods for calculating the optimal-fill charge, the height and the temperature of the coolant liquid for a V-shaped microgrooved heat pipe are presented using a macroscopic approach. The fill charge is determined to be an important parameter for the optimal performance of a heat pipe. The under- and overcharged heat pipes are less efficient than the optimally charged one. The worsening effect of the overcharge is more pronounced than the undercharge. The variation in the coolant liquid temperature is greater than that of the substrate temperature. In the sensitivity analysis of a micro heat pipe, under transient operation, the variations in the thermophysical properties, gravity force, and design parameters are considered. The present study sets forth both the qualitative and the quantitative effects of the variation in thermophysical properties of the coolant liquid and the design parameters of a V-shaped groove. These studies are carried out by solving the coupled nonlinear governing partial differential equations for fluid flow, heat transfer, and mass transfer using the finite-difference technique. © 2006 American Institute of Chemical Engineers *AIChE J,* 52: 3041–3054, 2006
Keywords: fill charge, grooved heat pipe, transient modeling, sensitivity analysis

Introduction

Recent advances in chip technology, which increases the component density, have spurred investigations of the thermal management problem in small electronic devices. The increased requirement for heat removal cannot be met by conventional methods. Two-phase heat transfer is a promising solution to this problem because of its high efficiency, reliability, and cost effectiveness. Therefore, micro-grooved heat pipes, using two-phase heat transfer, have become one of the most promising cooling devices. Recently, applications of micro heat pipes have extended from the thermal control of integrated electronic circuits packaging, laser diodes, photovoltaic cells, infrared (IR) detectors, and space vehicles to the removal of heat from the leading edges of stator vanes in turbines and nonsurgical treatment of cancerous tissue. To ensure wide applicability of a micro heat pipe, the present paper contributes in the following ways:

- First, it specifies the amount of coolant liquid to be charged in a micro-heat pipe and the adverse effects of either over- or undercharging, which are helpful for a heat pipe operation.
- Second, this analysis presents the sensitivity analysis of the system by varying (1) the design parameters, which guide the design of a heat pipe; and (2) the thermophysical properties of a heat pipe, which are helpful in selecting a proper coolant liquid.
- Third, the article evaluates the liquid height and liquid temperature, which aid in understanding the underlying phenomena of such a micro-system.

In a combination of these three benefits, the present study will be helpful for the start-up and the shutdown of a heat pipe operation.

We now overview the micro heat pipe literature. Cotter[1] first proposed the concept of a micro heat pipe as a wickless heat pipe for the uniform heat distribution in electronic chips. The

Correspondence concerning this article should be addressed to B. Suman at suman@cems.umn.edu.

micro heat pipe uses capillary pressure arising from the sharp corners of the groove in place of a wick. The microgrooved heat pipe is filled with a working fluid and the pipe is sealed. The heat flux is applied to a portion of the heat pipe, called the *evaporative section*, to vaporize the liquid. The vapor is pushed toward the condensing section, where heat is taken out. The capillary pressure difference between the evaporative and the condensing sections promotes the flow of the coolant fluid from the condenser to the evaporator. Suman and Hoda[2] showed that corners with sharp angles are necessary for an optimal heat pipe performance. Swanson and Herdt[3] showed that the change of pressure at the liquid–vapor interface leads to a greater variation in the profile of the meniscus. Thus, the flow of fluid is primarily governed by the pressure difference at the liquid–vapor interface.

Micro heat pipes can be embedded directly onto the silicon substrate of an integrated circuit, given that the effective thermal conductivity of a micro heat pipe has been estimated to be about tenfold that of the silicon substrate.[4] Mallik and Peterson[5] showed that for a non-steady-state thermal performance, micro heat pipes in silicon can reduce the thermal time constant by $>30\%$ compared to that of the plain silicon wafers. Peterson et al.[6] showed that the meniscus recession in the evaporator region causes a reduction in the meniscus curvature radius, which in turn causes an increase in the capillary pumping pressure. Babin et al.[7] developed a simplified numerical model and conducted experiments for measuring the maximum heat transport rate of a micro heat pipe. Wu and Peterson[8] numerically investigated the transient behavior of a micro heat pipe and compared their numerical results for the maximum heat transport rate in steady-state operation with the experimental data of Babin et al.[7]

A detailed thermal analysis and various limitations of a micro heat pipe were studied by Khrustalev and Faghri.[9] They developed a numerical model for heat and mass transfer in a micro heat pipe with triangular grooves by considering the thermal resistances in condensing and evaporative sections of the heat pipe. The results showed that the liquid–vapor interfacial shear stress and the contact angle could significantly influence the maximum heat transport rate of micro heat. Xu and Carey[10] developed an analytical model for evaporation from a V-shaped microgrooved surface, assuming that the evaporation takes place only from the thin film region of the meniscus. The model related the heat transfer in the microgroove to the fluid properties, groove geometry, and the constants for the disjoining pressure relation. Their predicted results were successfully compared with the experimental data. Catton and Stores[11] presented a one-dimensional semianalytical model for the prediction of wetted length in an inclined triangular capillary groove. They introduced the concept of *accommodation theory* to determine the change in the radius of curvature at the liquid–vapor interface. Suman et al.[12] presented a generalized steady-state model of a microgrooved heat pipe of polygonal shape. Suman and Kumar[13] developed an analytical model for the fluid flow and the heat transfer in a polygonal micro heat pipe. Their analytical model presents the analytical expressions for as critical heat input dry-out length and so on.

The amount of coolant liquid to be charged in a micro heat pipe, known as the *fill charge*, has a significant effect on the heat pipe performance. Tio et al.[14] and Ochterbeck[15] showed that a micro heat pipe works effectively at a given operating temperature and heat input if the fill charge is optimal. Duncan and Peterson[16] performed charged optimization of a microgrooved heat pipe and observed that with an increase in charging, the performance of a heat pipe increases. Because the flow of fluid in a micro heat pipe is attributed to the capillary pressure generated because of the radius of curvature, the optimal fill charge is not easily determined. Therefore, in this work a method for calculating optimal fill charge of the coolant liquid is proposed and the adverse effects of over- and undercharge are discussed in detail. The variation in the coolant liquid height under transient operation is also presented. The temperature difference between the substrate and the coolant liquid depends on the thermal resistance of the coolant liquid as the heat is being transferred along the liquid pool. The coolant liquid temperature determines the rate of condensation and evaporation.[17] Therefore, the temperatures of coolant liquid under transient and steady-state operations have been calculated.

Thus far, the sensitivity analysis of a micro heat pipe under transient operation has not been explored, although few transient models for a heat pipe are available in the literature. Transient mathematical models and experimental investigations for the wicked heat pipe have been reported in the literature.[18-26] Recently, the transient model for micro heat pipe was reported by Suman et al.[27] and Suman and Hoda.[28] However, the effects of variations in the thermophysical properties, design parameters, and gravitational acceleration remained uninvestigated. Therefore, the sensitivity analysis of the transient model for fluid flow and heat transfer is also presented in this study.

Theory

A V-shaped microgrooved heat pipe is considered in this study. A schematic of the heat pipe showing groove geometry is shown in Figure 1a. A V-shaped micro heat pipe showing the heat and fluid flow is presented in Figure 1b. The hot and the cold end are specified as the farthest end of the evaporative and the condenser region, respectively.

Model equations

The governing equations used in this work were taken from Suman et al.[27]. Although the model uses few assumptions, they have nonetheless been successfully compared from the experimental study.[27] The following assumptions were used in derivation of the governing equations:

(1) One-dimensional unsteady incompressible flow along the length of heat pipe; it has been shown that the flow along the transition region is small.[29]

(2) Heat dissipation resulting from viscosity is neglected.

(3) Flow arising from the surface tension gradient is neglected.

(4) Constant pressure in vapor region is taken, a valid assumption in this case because the vapor flow space in the channels is quite large, especially considering the low heat fluxes used in this study. The vapor pressure drop required for flow was calculated and determined to be very small.

(5) Negligible shear stress at the liquid–vapor interface, given that the channel area for vapor flow is relatively large and

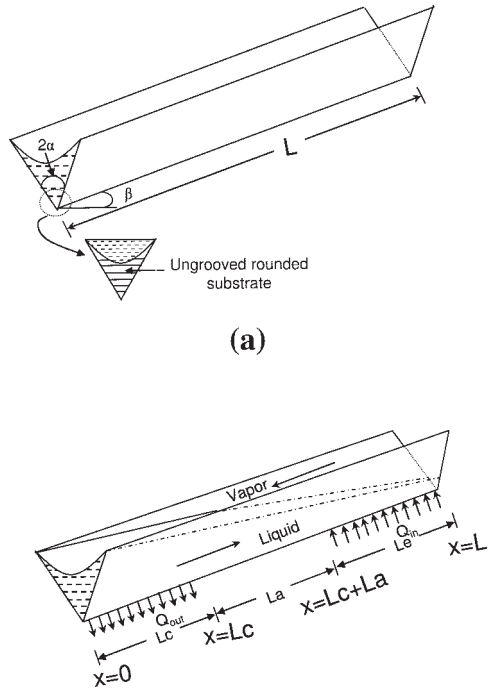

Figure 1. Micro heat pipe showing (a) groove geometry and (b) flow directions.

at the low heat fluxes used in this study the vapor velocity will generally be small. This justifies the assumption of no shear at the liquid–vapor interface.[8,30]

(6) Predefined steady-state heat flux interaction between the substrate and the coolant liquid (Q_{ss}) with position used by the coolant liquid. The fluid flow is governed by the pressure difference between the hot and the cold ends. The vapor pressure affects both the evaporation and the condensation. However, a successful formulation of dependency of heat fluxes on vapor pressure has not been done. Therefore, in this work the predefined heat interaction between the substrate and the coolant liquid has been taken.[11,31]

(7) Convective heat loss is neglected because two-phase heat transfer is orders of magnitude higher than the natural convection.

A Δx length of a V-shaped microgrooved heat pipe is taken as the control volume, which is shown in Figure 2. Although the governing equations are similar to those presented in Suman et al.,[27] we briefly discuss them here. The variation of pressure with time and position is given by Young–Laplace equation, which is in differential form, and is read as

$$\frac{\partial P_l}{\partial x} = \frac{\sigma_l}{R^2}\frac{\partial R}{\partial x}, \tag{1}$$

where $\partial P_l/\partial x$ and $\partial R/\partial x$ are the pressure and the radius of curvature gradient, respectively.

The differential form of the unsteady state momentum balance is expressed as

$$\rho_l A_l V_l \frac{\partial (V_l)}{\partial x} + A_l \frac{\partial P_l}{\partial x} + 2L_h \tau_w - \rho_l g \sin\beta A_l + \frac{\partial (\rho_l A_l V_l)}{\partial t} = 0. \tag{2}$$

The expressions for R_m, substrate half-wetted length (L_h), and the liquid area (A_l) can be obtained from the groove geometry and are presented in the Appendix.

The differential form of the unsteady mass balance of the coolant liquid is

$$\frac{\partial (\rho_l A_l)}{\partial t} + \frac{\partial (\rho_l A_l V_l)}{\partial x} + \frac{Q_v R_m}{\lambda_l} = 0. \tag{3}$$

Similarly, the differential form of the unsteady state mass balance of the vapor is given as

$$\frac{\partial (\rho_g A_g)}{\partial t} + \frac{\partial (\rho_g A_g V_g)}{\partial x} - \frac{Q_v R_m}{\lambda_l} = 0. \tag{4}$$

Keblinski et al.[32] reported that the thermal conductivity of the coolant liquid can be increased manyfold and thus the energy balance equation for the coolant liquid of the existing model[27] has been modified and the following equation was obtained by considering the conduction in the coolant liquid:

$$\rho_l C_{pl} A_l \frac{\partial T_l}{\partial t} + \rho_l C_{pl} V_l A_l \frac{\partial T_l}{\partial x} - K_l \frac{\partial}{\partial x}\left\{A_l \frac{\partial T_l}{\partial x}\right\} - Q w_b + Q_v R_m = 0. \tag{5}$$

where Q is the heat interaction between the coolant liquid and the solid substrate.

The variable Q is positive in the evaporative section because it is taken by the coolant liquid and it is negative in the condenser region, where it is released by the coolant liquid to the substrate. It is zero in the adiabatic section because there is no heat interaction between the coolant liquid and the solid substrate. The unsteady state energy balance in the substrate is given as

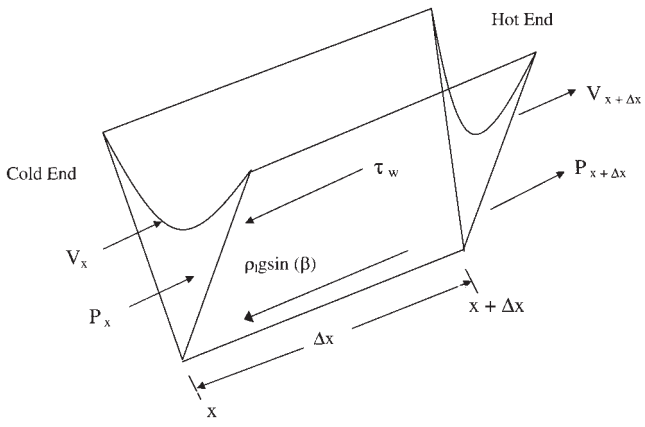

Figure 2. Volume element of a V-shaped microgrooved heat pipe with all forces specified.

$$A_{cs}K_s\frac{\partial^2 T_s}{\partial x^2} - Qw_b - \rho_s C_{p_s} A_{cs}\frac{\partial T_s}{\partial t} = 0. \qquad (6)$$

We now discuss the heat interaction between the substrate and the coolant liquid with time. The heat supplied by the heater is first conducted through the solid substrate, and then the heat is taken up by the coolant liquid in the evaporative section. The heat is transferred by two-phase heat transfer mechanism, that is, evaporation. Similarly, the vapor is condensed in the condensing section and the released heat is being taken up by the solid substrate. No exchange of heat between the solid substrate and the coolant liquid has been considered in the adiabatic section. Initially, the supplied heat by the heater is used to raise the temperature of the substrate and the heat interaction between the coolant liquid and the solid substrate is diminished. With an increase in time, the heat interaction between the coolant liquid and the solid substrate increases because the heat used to raise the temperature of the solid substrate decreases. This phenomenon can be approximated to the situation of the transient heat conduction problem with the external heat removal. Therefore, the heat interaction between the substrate and the coolant liquid is approximated using a lump capacity model and the exponential variation of the heat interaction between the coolant liquid and the solid substrate has been assumed. The part of heat that is not being used by the coolant liquid is considered to be used in heating of the substrate. Thus, the heat flux taken up or released by the coolant liquid is given as

$$Q = Q_{ss}(1 - e^{-t/\tau}). \qquad (7)$$

where Q_{ss} is the heat flux interaction between the substrate and the coolant liquid at the steady state; the quantity Q is the heat flux used or released by the coolant liquid to the substrate at any time t; and the quantity τ is a time constant, defined as $\tau = \rho_s C_{ps} L^2/K_s$, which is a characteristic time for the heat transfer in the substrate.

Initial and boundary conditions

The boundary conditions at the cold end ($x = L$) are

$$R = R_o, \qquad P_l = P_{v_o} - \frac{\sigma_l}{R_o}, \qquad T_s = T_{con},$$
$$V_l = 0, \qquad V_g = 0, \qquad \forall\, t.$$

The quantity R_o is the radius of curvature at the cold end, which can be obtained from the groove geometry and is presented in the Appendix. The temperature at the end of the condenser region, T_{con}, is taken to be 32°C.

At the hot end ($x = 0$), the boundary condition is

$$Q_{heater} = -K_s A_{cs}\left.\frac{\partial T_s}{\partial x}\right|_{x=0}, \qquad \forall\, t.$$

The initial conditions (at $t = 0$) are

$$T_s = T_{con}, \qquad V_l = 0, \qquad P_l = P_{v_o} - \frac{\sigma_l}{R_o} - \rho_l g(L - x)\sin\beta,$$
$$R = \frac{\sigma_l}{(P_{v_o} - P_l)}, \qquad \forall\, x.$$

Nondimensionalization

The constant parameters used in the nondimensionalization are as follows: reference velocity = $V_R = Q_{ss}/\rho_l R_o^2 \lambda_l$ =0.0016 m/s), reference pressure = $P_R = \sigma_l/R_o$ (=148.1 N/m^2), reference height h_R, expressed as

$$h_R = R_o\left[\frac{\cos(\alpha+\gamma)}{\tan\alpha} + \sin(\alpha+\gamma) - 1\right]$$
$$(=1.1547 \times 10^{-4}\ \text{m})$$

reference temperature = $T_R = T_{con}$ (32°C), reference axial length = L (2 cm), reference radius of curvature = R_o (=1.1547 × 10^{-4} m), and time constant = $\tau = \rho_s C_{ps} L^2/K_s$ (=0.2269 s). The position-varying parameters are as follows: friction factor = $f = K'/N_{\mathrm{Re}}$ (13.33), where K' depends on the groove geometry, Reynolds number = $N_{\mathrm{Re}} = D_h \rho_l V_l/\mu_l$, hydraulic diameter = $D_h = 4A_l/2L_h$, and wall shear stress = $\tau_w = \rho_l V_l^2 f/2$.

The dimensionless parameters are defined as follows: dimensionless radius of curvature = $R^* = R/R_o$, dimensionless position = $X^* = x/L$, dimensionless liquid velocity = $V_l^* = V_l/V_R$, dimensionless vapor velocity = $V_g^* = V_g/V_R$, dimensionless liquid pressure = $P_l^* = P_l/P_R$, dimensionless substrate temperature = $T_s^* = T_s/T_R$, dimensionless height = $h^* = h/h_o = R^*$, and dimensionless time = $t^* = t/\tau$. Dimensionless forms of the heat and mass transfer and fluid flow equations are as follows:

$$\frac{\partial P_l^*}{\partial X^*} = \frac{1}{R^{*2}}\frac{\partial R^*}{\partial X^*}, \qquad (8)$$

$$\frac{\partial R^*}{\partial t^*} = -\left[\frac{\tau R^* Q_v R_m L}{2\rho_l A_l \lambda_l} + \frac{2\tau V_R V_l^*}{LR^*}\frac{\partial R^*}{\partial X^*} + \frac{\tau R^* V_R}{2L}\frac{\partial V_l^*}{\partial X^*}\right], \qquad (9)$$

$$\frac{\partial V_l^*}{\partial t^*} = \frac{\tau g\,\sin(\beta)}{V_R} + \frac{\tau Q_v R_m V_l^*}{A_l \rho_l \lambda_l} - \frac{\tau B_2 V_l^*}{\rho_l (R_o R^*)^2} - \left[\frac{\tau\sigma_l}{\rho_l V_R R_o L R^{*2}} - \frac{2\rho_l \tau V_R V_l^{*2}}{LR^*}\right]\frac{\partial R^*}{\partial X^*}, \qquad (10)$$

$$\frac{\partial V_g^*}{\partial X^*} = -\frac{Q_v R_l L}{\rho_l A_g \lambda_l V_R} + \frac{2A_l V_g^*}{A_g R^*}\frac{dR^*}{dX^*} + \frac{2A_l}{\tau\rho_l A_g V_R R^*}\frac{\partial R^*}{\partial t^*}, \qquad (11)$$

$$\frac{\partial T_s^*}{\partial t^*} = \frac{\partial^2 T_s^*}{\partial X^{*2}} - \frac{Qw_b L^2}{T_R A_{cs} K_s}, \qquad (12)$$

$$Q = Q_{ss}(1 - e^{-t^*}), \qquad (13)$$

$$Q_V = \frac{1}{R_m}\left[Qw_b - \frac{\rho_l C_{pl} V_R V (A_l T_R}{L}\frac{\partial T_l^*}{\partial X^*} - \rho_l C_{pl} A_l T_R \tau \frac{\partial T_l^*}{\partial t^*}\right] + \frac{1}{R_m}\left[+ K_l B_1 \left\{ \frac{2R^* R_o^2 T_R}{L^2}\frac{\partial R^*}{\partial X^*}\frac{\partial T_l^*}{\partial X^*} + \left(\frac{R(R_o T_R}{L}\right)^2 \frac{\partial^2 T_l^*}{\partial X^{*2}}\right\}\right], \quad (14)$$

where A_l, w_b, R_m, B_1, and B_2 are defined in the Appendix.

The above set of dimensionless equations (Eqs. 8–14) was solved numerically by taking predefined heat flux interaction between the substrate and the coolant liquid along the heat pipe length. The variable Q is constant with position in this study. Boundary conditions at the cold end ($X^* = 0$) are

$$R^* = 1, \qquad P_l^* = \frac{P_{v_o}}{P_R} - 1, \qquad V_l^* = 0,$$

$$T_s^* = \frac{T_{con}}{T_R}, \qquad \forall\, t^*.$$

The boundary condition at the hot end ($X^* = 1$) is

$$Q_{heater} = -\frac{K_s A_{cs} T_R}{L}\left.\frac{\partial T_s^*}{\partial X^*}\right|_{X^*=0}, \qquad \forall\, t^*.$$

Initial conditions (at $t^* = 0$) are

$$T_s^* = \frac{T_{con}}{T_R}, \qquad V_l^* = 0,$$

$$P_l^* = \frac{P_{v_o}}{P_R} - 1 - \frac{\rho_l g L(1 - X^*)\sin(\beta)}{P_R},$$

$$R^* = \frac{P_R}{(P_{v_o} - P_R P_l^*)}, \qquad \forall\, X^*.$$

Fill charge

The amount of coolant liquid to be charged in a micro heat pipe, known as *fill charge*, has a significant effect on the heat pipe performance.[15,16] The fill charge m_f can be calculated from the following equation:

$$m_f = \rho_l L \int_0^1 A_l dX^* + \rho_g L \int_0^1 A_g dX^* = (\rho_l - \rho_g) L B_1 R_o^2 \int_0^1 (R^*)^2 dX^* + \rho_g A_{cs} L. \quad (15)$$

Expanding the above equation into the three contributions to the fill charge yields the following expression:

$$m_f = \underbrace{\rho_l L \int_0^{L_f^*} A_l dX^* + \rho_g L \int_0^{L_f^*} A_g dX^*}_{\text{Flooded region}} + \underbrace{\rho_l L \int_{L_f^*}^{1-L_d^*} A_l dX^* + \rho_g L \int_{L_f^*}^{1-L_d^*} A_g dX^*}_{\text{Operating region}} + \underbrace{\rho_g L \int_{1-L_d^*}^{1} A_g dX^*}_{\text{Dry region}}. \quad (16)$$

A further simplification is expressed as

$$m_f = \rho_l L B_1 R_o^2 \int_0^{L_f^*} dX^* + \rho_g L (A_{cs} - B_1 R_o^2) \int_0^{L_f^*} dX^* + \rho_l L B_1 R_o^2 \int_{L_f^*}^{1-L_d^*} R^{*2} dX^* + \rho_g L \int_{L_f^*}^{1-L_d^*} (A_{cs} - B_1 R_o^2 R^{*2}) dX^* + \rho_g L \int_{1-L_d^*}^{1} A_{cs} dX^*. \quad (17)$$

Here, B_1 is a geometrical parameter whose expression is given in the Appendix. From Eq. 16, we see that the fill charge has three contributions: first from the flooded region, second from the operating region, and third from the dry-out length region. It is to be noted that the contribution from the flooded region and the dry-out region deteriorates the performance of the pipe and we always aim to minimize the flooded and the dry-out length. If the coolant liquid is overcharged, a portion of the condensing section is flooded and it increases the liquid pool thickness. An increase in the liquid pool thickness increases the heat transfer resistance of the coolant liquid. Flooding in a portion of the condenser leads to a smaller condenser section and thus a higher rate of heat removal from the condenser region is required. If the coolant liquid is undercharged, the area available for the flow of the liquid is diminished. This increases the liquid velocity, resulting into a higher frictional loss. Additionally, the coolant liquid available for the evaporation is less and thus the onset of the dry-out is expected to occur at a lower heat input.

Optimal-fill charge

The optimal-fill charge is the amount of coolant liquid required to meet the boundary conditions, $R^* = 1$ at $X^* = 0$, at a particular heat input, without generating any hot spot (that is, $R^* = 0$ at $X^* = 1$). In other words, the lengths of the flooded and the dry regions are zero, and the cold end is completely filled, that is, $R^* = 1$ at $X^* = 0$ and $R^* = 0$ at $X^* = 0$. An optimally charged micro heat pipe is presented in Figure 3. The expression for the optimal fill charge is given as

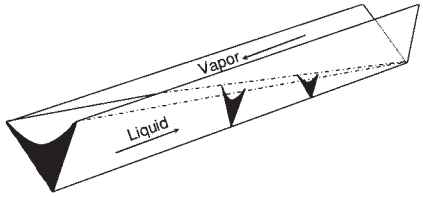

Figure 3. An optimally charged micro heat pipe.

$$m_f = \underbrace{\rho_l L \int_0^1 A_l dX^* + \rho_g L \int_0^1 A_g dX^*}_{\text{Flooded region}}$$

$$= \rho_l L B_1 R_o^2 \int_0^1 R^{*2} dX^* + \rho_g L \int_0^1 (A_{cs} - B_1 R_o^2 R^{*2}) dX^*. \tag{18}$$

The optimal-fill charge was calculated using numerical integration to solve Eq. 18. The dimensionless radius of curvature (R^*) as a function of X^*, which satisfies $R^* = 1$ at $X^* = 0$ at a particular heat input, can be calculated by solving dimensionless Eqs. 8 to 14. Equation 18 along with the dimensionless model (Eqs. 8 to 14) suggests that the optimal charge increases with an increase in heat input, contact angle, and length of heat pipe; and decreases with an increase in inclination, acceleration arising from gravity, and surface tension.

Overcharge

A heat pipe is overcharged if the amount of the coolant liquid poured into a heat pipe is greater than the optimal charge. In this case, the coolant liquid in the heat pipe can be accommodated in three ways. In the first case, we have a flooded region and second case, $R^* > 0$ at $X^* = 1$; and third is a combination of first and second cases. In all three cases, the length of the dry region is zero. An overcharged micro heat pipe for first and second situations is shown in Figure 4. The expression for the fill charge of an overcharged heat pipe becomes

$$m_f = \underbrace{\rho_l L \int_0^{L_f^*} A_l dX^* + \rho_g L \int_0^{L_f^*} A_g dX^*}_{\text{Flooded region}}$$

$$+ \underbrace{\rho_l L \int_{L_f^*}^{1-L_d^*} A_l dX^* + \rho_g L \int_{L_f^*}^{1-L_d^*} A_g dX^*}_{\text{Operating region}}$$

$$= \rho_l L B_1 R_o^2 \int_0^{L_f^*} dX^* + \rho_g L (A_{cs} - B_1 R_o^2) \int_0^{L_f^*} dX^*$$

$$+ \rho_l L B_1 R_o^2 \int_{L_f^*}^1 R^{*2} dX^* + \rho_g L \int_{L_f^*}^1 (A_{cs} - B_1 R_o^2 R^{*2}) dX^*. \tag{19}$$

The overcharge of the coolant liquid deteriorates the performance of a heat pipe. In this case, a portion of the condenser region has $R^* = 1$ rather than $R^* = 1$ only at the cold end or $R^* > 0$ at $X^* = 1$. In both cases, the coolant liquid thickness is greater than the coolant liquid thickness for the optimal charge. This increases the resistance for the heat transfer across the coolant liquid. Higher thermal resistance requires higher a temperature drop between substrate and coolant liquid to conduct the same amount of heat. Therefore, the coolant temperature is relatively lower in the evaporative section and is relatively higher in the condenser section. This decreases the evaporative heat flux[17] and the condensing heat flux. However, this effect has not been considered in the present work. The heat dissipation on the substrate takes place because the required amount of heat is not transferred. On the other hand, a portion of the condenser region is flooded and thus a higher heat flux removal is required in the condensing region.

To achieve a quantitative effect of the overcharge, the following procedure has been developed. When a portion of the condensing section, L_f^*, is flooded, that is, $R^* = 1$ at $X^* \le L_f^*$, then the new set of initial conditions (at $t^* = 0$) is given as

$$T_s^* = \frac{T_{con}}{T_R}, \quad V_l^* = 0, \quad P_l^* = \frac{P_{v_o}}{P_R} - 1 - \frac{\rho_l g L (L_f^* - X^*) \sin(\beta)}{P_R},$$

$$R^* = \frac{P_R}{(P_{v_o} - P_R P_l^*)}, \qquad \forall\, X^*.$$

Using the new set of initial conditions and the amount of mass charged in a heat pipe, the value of L_f^* for that particular fill charge can be obtained. The new set of boundary conditions at $X^* = 0$ shifts to the new location, $X^* = L_f^*$. The new set of boundary conditions at $X^* = L_f^*$ is given as

$$R^* = 1, \qquad P_l^* = \frac{P_{v_o}}{P_R} - 1, \qquad T_s^* = \frac{T_{con}}{T_R}, \qquad \forall\, t^*.$$

The governing Eqs. 8 to 14 can be solved using above boundary and initial conditions to study the overcharge of a heat pipe in a flooded condition.

When $R^* > 0$ at $X^* = 1$, but a portion of a heat pipe is not

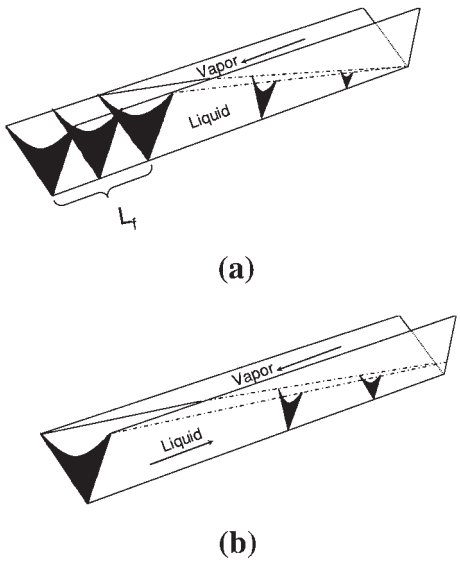

Figure 4. An overcharged micro heat pipe (a) when a potion of a heat pipe is completely filled and (b) when a heat pipe is completely filled at the cold end.

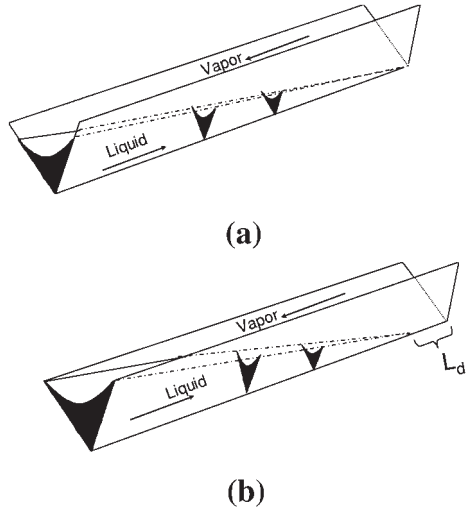

Figure 5. An undercharged micro heat pipe (a) when a heat pipe does not have a dry region and (b) when a heat pipe has a dry region.

flooded, the initial condition and the boundary conditions do not change as in the case above; however, we do not have $R^* = 0$ at $X^* = 1$ and this results in an increase in liquid pool thickness and its adverse effect has been explained above.

Undercharge

A heat pipe is undercharged if the amount of coolant liquid poured into the heat pipe is less than the optimal charge. An undercharge of a coolant liquid can lead to three situations: (1) the quantity R^* reaches a value $f_u < 1$, at $X^* = 0$; or (2) a portion of the heat pipe is dry, that is, $R^* = 0$ at $X^* = 1 - L_d^*$, and $R^* = 1$ at $X^* = 0$ or combination of (1) and (2). An undercharged heat pipe for situations (1) and (2) is shown in Figure 5. The expression for the fill charge of an undercharge heat pipe becomes

$$m_f = \underbrace{\rho_l L \int_0^{1-L_d^*} A_l dX^* + \rho_g L \int_0^{1-L_d^*} A_g dX^*}_{\text{Operating region}} + \underbrace{\rho_g L \int_{1-L_d^*}^{1} A_g dX^*}_{\text{Dry region}}$$

$$= \rho_l L B_1 R_o^2 \int_0^{1-L_d^*} R^{*2} dX^* + \rho_g L \int_0^{1-L_d^*} (A_{cs} - B_1 R_o^2 R^{*2}) dX^* + \rho_g L \int_{1-L_d^*}^{1} A_{cs} dX^*. \quad (20)$$

If the heat pipe has a dry region, it does not work properly unless an additional amount of the coolant liquid is charged. If R^* reaches a value $f_u < 1$, at $X^* = 0$, it results in three adverse effects. First, less coolant liquid has a smaller liquid area, which increases the liquid velocity for the same heat input, resulting in a higher frictional loss. Second, less liquid is available for the evaporation and thus the dry out occurs at a lower heat input. Third, $R^* \neq 1$ at $X^* = 0$ and thus a portion of the groove is not used for the two-phase heat transfer.

To calculate a quantitative measurement of the effect of the undercharge, the following procedure has been developed. We assume that R^* reaches a value $f_u < 1$, at $X^* = 0$, and thus the initial conditions (at $t^* = 0$) have been changed as follows:

$$T_s^* = \frac{T_{con}}{T_R}, \quad V_l^* = 0, \quad P_l^* = \frac{P_{v_o}}{P_R} - \frac{1}{f_u} - \frac{\rho_l g L (1 - X^*) \sin(\beta)}{P_R},$$

$$R^* = \frac{P_R}{(P_{v_o} - P_R P_l^*)}, \quad \forall\, X^*.$$

Using the new set of initial conditions and the amount of mass charged in heat pipe, the value of f_u for that particular fill charge can be obtained. The new set of boundary conditions at the cold end ($X^* = 0$) can be given as

$$R^* = f_u, \quad P_l^* = \frac{P_{v_o}}{P_R} - \frac{1}{f_u}, \quad T_s^* = \frac{T_{con}}{T_R}, \quad \forall\, t.$$

The governing Eqs. 8 to 14 should be solved using above boundary and initial conditions to study the undercharge for $R^* = f_u$, at $X^* = 0$. If a portion of the heat pipe is dry, it means the heat pipe has reached its limit and cannot be used for the purpose of cooling.

Coolant liquid height

The coolant liquid height (h) is defined as the maximum thickness of the coolant liquid pool. The variation of coolant liquid pool with time and position can be shown by calculating the liquid height from the following equation:

$$h = R\left[\frac{\cos(\alpha + \gamma)}{\tan \alpha} + \sin(\alpha + \gamma - 1)\right] \quad (21)$$

where R is the radius of curvature, α is the half-groove angle, and γ is the contact angle. Using the reference height,

$$h_R = R_o\left[\frac{\cos(\alpha + \gamma)}{\tan \alpha} + \sin(\alpha + \gamma) - 1\right],$$

the above expression for the liquid height has been nondimensionalized. The nondimensional equation is as follows:

$$h^* = R^*. \quad (22)$$

From Eq. 21 it can be seen that the coolant liquid height depends on the contact angle of the coolant liquid-substrate system, the radius of curvature, and the groove geometry. The coolant liquid pool contributes significantly to the heat transfer resistance of a heat pipe. Therefore, the coolant liquid height should be considered while designing a micro heat pipe.

Coolant liquid temperature

The liquid temperature was calculated based on a predefined rate of evaporation and condensation and liquid thermal resis-

tance. The temperature difference between the substrate and the coolant liquid depends on the thermal resistance of the coolant liquid. The temperature of the midpoint of the coolant liquid was calculated and it can be extrapolated/interpolated to calculate the coolant liquid temperature at any location in liquid pool. The coolant liquid temperature at the midpoint was evaluated as described below.

The heat is transferred to the coolant liquid from the substrate. Therefore, $Qw_b = Q_l L_h$, where Q_l is the heat flux at the solid–liquid interface. The average heat flux, Q_{avg}, through the coolant liquid, $(Q_l + Q_v)/2$, can be assumed at the midpoint of the coolant liquid pool. The quantity Q_v is the heat flux at the liquid–vapor interface. The thermal resistance of the coolant liquid at the midpoint has been given by $R_{th} = (A_l/2L_h)/K_l$. The equation of heat conduction along the liquid pool gives the dimensionless temperature at the midpoint of the coolant liquid as

$$T_l^* = T_s^* - \frac{Q_{avg} R_{th}}{T_R} \tag{23}$$

Performance factor of micro heat pipe

The performance factor gives the quantitative measurement of the performance of a micro heat pipe. It is obtained while presenting the analytical expression for the radius of the curvature, the critical heat input, and the dry-out length. It is based on the heat transfer limit in the heat pipe rather the effective thermal conductivity of a heat pipe. The performance factor, B, has been defined as[13]

$$B = \frac{\sigma R_0^3 \rho_l \lambda B_1}{B_2 L Q_{in}}. \tag{24}$$

This expression captures the property of the coolant liquid using surface tension, viscosity (in B_2), contact angle (in B_2), density, and latent heat of vaporization. As is clear from the expression, with the higher latent heat of vaporization, density, and surface tension, the performance factor increases whereas with an increase in viscosity, it decreases. Thus, it is used to study the performance of a heat pipe when the thermophysical properties of a coolant liquid change. The performance factor also has some geometric constants, such as B_1, B_2, and L, which measure the effect of the geometric parameters. Like the performance factor is proportional to B_1, which measures the liquid accommodation capacity of a heat pipe. The performance of a heat pipe increases with B_2. The higher the heat pipe length, the lower the performance factor. This is explained by the fact that with an increase in the length of a heat pipe, the frictional loss increases. Thus, the performance factor measures the effect of geometric parameters as well.

The higher the value of the performance factor, the better the performance of a heat pipe, that is, a higher critical heat input. Thus, a combination of thermophysical properties of the coolant liquid, design parameters, and contact angle of the liquid-substrate system that gives a higher value of B should be chosen for a fixed heat input. Therefore, it is suggested that the value of B should be considered while designing a micro heat pipe.

Numerical solution

A set of partial differential and algebraic equations (Eqs. 8 to 14) were converted into a system of differential algebraic equations using the finite-difference method. The first-order spatial derivative was estimated using either a forward- or a backward-differencing method based on the flow direction. The second derivatives were estimated using a central-differencing method. The Neumann boundary conditions were attended to by using ghost boundary nodes. Equation 12 is not coupled to Eqs. 9 and 11 and thus it was solved first for a given time step using the Newton–Raphson method. The differential equations corresponding to Eqs. 9 and 11 were solved in a coupled manner using a pseudoimplicit method, which helps in taking large time steps without affecting the convergence. A set of algebraic equations was obtained based on the above discretization scheme. The set of algebraic equations for Eqs. 9 and 11 was solved simultaneously by using the Newton–Raphson method with the obtained temperature profile from solution of Eq. 12. The dimensionless step sizes for spatial and temporal discretization used are 0.2 and 0.1, respectively.

Results and Discussion

The transient operation and its sensitivity analysis of a V-shaped micro heat pipe have been presented. A silicon substrate (0.8 cm wide and 2.3 cm long) has been considered. A portion of the length, 0.3 cm, is not grooved because it is used by the heater to supply heat to the system. Thus, the effective length of a heat pipe is 2 cm. The lengths of the evaporative, the adiabatic, and the condenser regions are assumed to be equal. The width and the spacing of a V-groove are taken as 0.2 mm. The apex angle of a V-groove is 60°. A set of 100 such grooves have been considered in this study. The temperature at the condenser end and the reference temperature were taken as 32°C. The inclination of the heat pipe is 10°. A constant heat interaction between the coolant liquid and the substrate was assumed. Pentane and silicon were chosen as the working fluid and the substrate, respectively. The contact angle was zero unless another value is specified.

Fill charge

The fill charge of coolant liquid, the performance factor of the heat pipe, the time to reach steady state, the initial and the steady-state values of dimensionless radius of curvature at $X^* = 0.5$, and the liquid resistance at X^* values of 0.25, 0.5, and 0.75 are detailed in Table 1. Three fill charges have been considered, one for each case (optimal-, under-, and overcharge). The radius of curvature with time monotonically decreases with time for each case and the initial and the steady-state values for dimensionless radius of curvature $X^* = 0.5$ are also given in Table 1. From this table, it can be concluded that the undercharge deteriorates the performance of the heat pipe. No difference in the performance factor of a microgrooved heat for the optimal- and the overcharge has been reported, given that the overcharge is not considered in the definition of performance factor. However, a portion of the condenser is not used and thus the required removal flux increases. The liquid thermal resistance is more for the overcharge because it has a higher liquid pool thickness and is less for the undercharge because it has a lower liquid pool thickness. A higher liquid

Table 1. Fill Charge and Performance Factor for Different Situations of Coolant Liquid Charging

	Undercharge	Optimal Charge	Overcharge
% Charging	86.5	100	101.23
Charged mass (mg)	7.91	8.14	8.21
Boundary/initial conditions	$R^* = 0.95$ at $X^* = 1$	$R^* = 1$ at $X^* = 1$	$R^* = 1$ at $X^* = 0.97$
R^* at $X^* = 0.5$ at $t^* = 0$	0.884	0.932	0.930
R^* at $X^* = 0.5$ at $t^* = 110.2$	0.776	0.832	0.832
t^* to reach steady state	77.12649	83.73	88.14
Performance factor	3.3758	3.9374	3.9374**

**The performance factor formula does not have the effect of overcharge.

resistance leads to a higher temperature drop between the substrate and the coolant liquid and thus less evaporative and condensing heat fluxes. Therefore, both over- and undercharge are not desirable. Additionally, the undercharge is not desired because dry-out occurs at a lower heat input and the frictional loss is more as a result of the higher liquid velocity. The time to reach steady state increases with an increase in fill charge. It is also obtained that the effect of the overcharge is worse than that of the undercharge because even a 1.2% increase in the optimal charge can deteriorate the performance of the heat pipe. In their experimental work Duncan and Peterson[16] found that with an increase in fill charge, the performance of a micro heat pipe increases. This result is consistent with that of the present model because initially the heat pipe is undercharged and as the charging increases, it approaches the optimal fill charge and the performance increases.

Coolant liquid height

The coolant liquid height as a function of time and position is shown in Figure 6. It is seen that the liquid pool thickness decreases with time because a part of the coolant liquid is evaporated. As time increases, the heat input increases and more liquid is evaporated, resulting in a decrease in the liquid height. The rate of change of the liquid height decreases with time as the heat input approaches its steady-state value. The variation in the liquid height with time is greater in the evaporative section because the amount of liquid required for evaporation, which has to flow from the condensing to the evaporative section, increases with time and it requires a higher liquid pressure, which results in a decrease in the liquid height in the evaporative section. The variation in the liquid height with position is more in the adiabatic section.

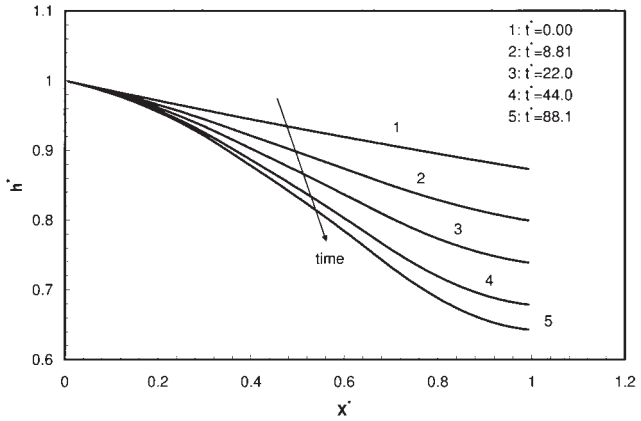

Figure 6. Variation in dimensionless liquid height with dimensionless position for different times for a heat input of 0.05 W.

Coolant liquid temperature

The temperature of the midpoint of the coolant liquid and the substrate as a function of time are shown in Figures 7a and 7b, respectively. It is seen that the time to reach the steady state is around ($t^*\tau$) 20 s, which is consistent with the experimental investigation for a micro heat pipe reported by Wu and Peterson.[8] A similar value for the flat heat pipe was reported by Wang and Vafai.[26] In the work by Wang and Vafai,[26] the time to reach steady state was found to be independent of heat input, which is obtained in the present work as well.

In Figures 7a and 7b, it is seen that the variation in the substrate temperature is smaller than that in the coolant liquid. The coolant temperature is lower than the substrate temperature in the evaporative section because heat is flowing from the substrate to the coolant liquid; it is higher than the substrate temperature in the condensing section because heat is flowing from the coolant liquid to the substrate. The liquid and the substrate temperatures remain the same in the adiabatic section, given that there is no flow of heat in the adiabatic section. The temperature difference between the substrate and the coolant increases with time as the heat input increases with time. It is also observed that the nature of the variation of the liquid temperature is different from that of the substrate. This is because that the liquid temperature is governed by the heat transfer between that substrate and the coolant liquid along the liquid pool, whereas the substrate temperature is governed by the conduction along the solid and heat interaction between the substrate and the liquid.

Temperatures of the midpoint of coolant liquid and the substrate as a function of position are shown in Figures 8a and 8b, respectively. This figure clearly shows that the coolant liquid temperature is lower than the substrate temperature in the evaporative section, the coolant liquid temperature is the same as the substrate temperature in the adiabatic section, and the temperature coolant liquid temperature is higher than the substrate temperature in the condensing section. The coolant liquid temperature undergoes a jump at the junction of both evaporative and adiabatic regions, and adiabatic and condensing sections. This is explained by the predefined constant heat transfer between the coolant and the substrate used for evaporation and condensation and no heat transfer between the coolant and the substrate in the adiabatic section. The difference in the coolant and the substrate temperatures is substantial and this encourages further study of this aspect for micro heat

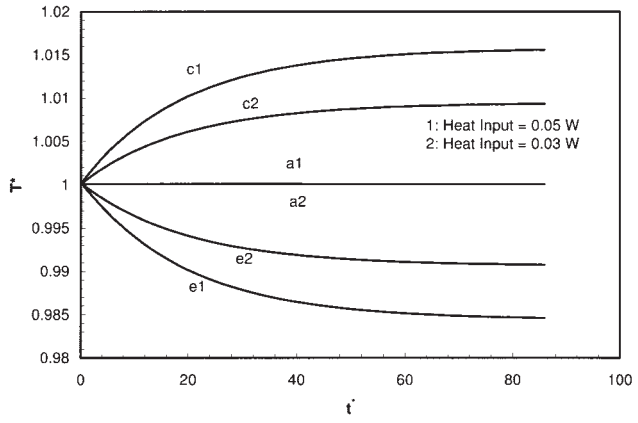

(a)

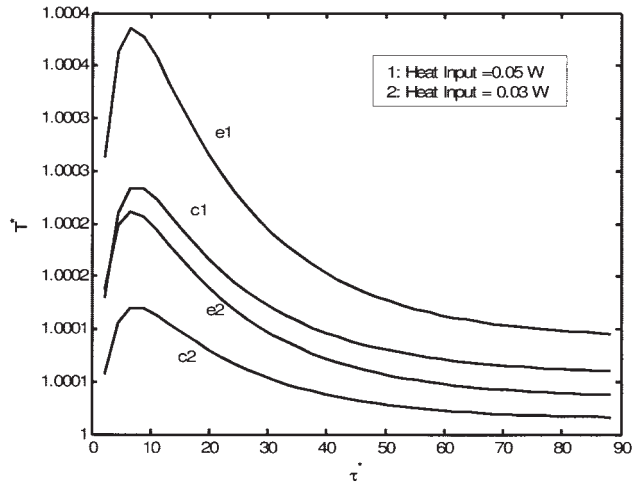

(b)

Figure 7. Variation of temperature vs. dimensionless time for (a) liquid and (b) substrate.

For both (a) and (b), the notation "c" denotes the position $X^* = 0.25$ in the condenser region, "e" denotes the position $X^* = 0.75$ in the evaporative region, and "a" denotes the position $X^* = 0.50$ in the adiabatic section.

pipe because evaporative and condensing fluxes constitute a function of liquid temperature, although it has not been considered in this work.

Effect of coolant liquid thermal conductivity

The effect of the thermal conductivity of the coolant liquid on the dimensionless radius of curvature as a function of time has been studied. The effect of the coolant liquid thermal conductivity was found to be insignificant, given that heat conduction through the coolant liquid along the heat pipe is less. This results from the small area available for heat flow and larger length. However, for a functional heat pipe, the thermal conductivity affects the condensation film and the evaporative film in the heat pipe; thus, it affects the heat transfer rate, the contact angle, and the radius of curvature at the liquid–vapor interface. However, it is has not been captured in the model presented herein because we have assumed the predefined heat interaction between the solid substrate and the coolant liquid. It is expected that the effect of the liquid thermal conductivity will be significant when the predefined heat flux in the evaporative and condensing sections will be removed. The heat fluxes in the evaporative and the condensing sections are functions of liquid temperature and with a higher thermal conductivity of coolant liquid, the temperature difference between the substrate and the coolant liquid will be less, which will enhance both the evaporative and the condensing heat fluxes. Therefore, the performance of a heat pipe will be improved.

Sensitivity analysis

The effect of gravity force on the transient behavior of a micro heat pipe has been studied by varying the acceleration arising from gravity and the inclination. The radius of curvature with time monotonically decreases with time for each case, and the initial and the steady-state values for the dimensionless radius of curvature $X^* = 0.5$ are given in Table 2. It is seen that with a higher opposing gravity force, the time to reach steady

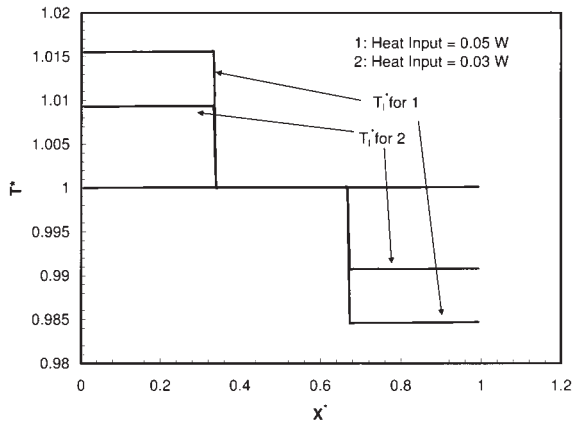

(a)

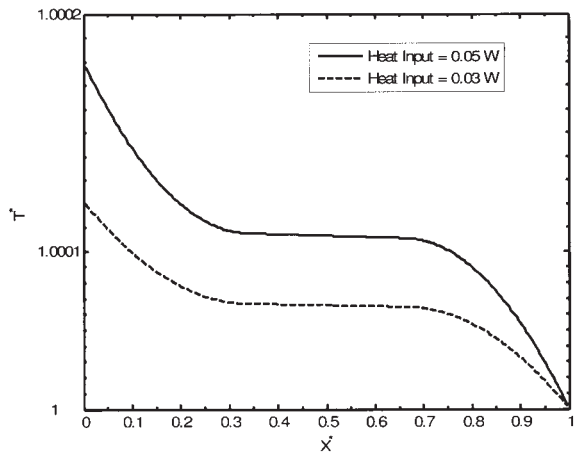

(b)

Figure 8. (a) Dimensionless liquid temperature vs. dimensionless position and (b) dimensionless substrate temperature vs. dimensionless position for different heat inputs.

Table 2. Effect of Gravity Force on the Transient Behavior of a Micro Heat Pipe

Parameter	Value	t^* to Reach Steady State	R^* at $X^* = 0.5$ at $t^* = 0$	R^* at $X^* = 0.5$ at $t^* = 110.2$
Inclination (β in °)	10°	83.74	0.932	0.832
	30°	88.14	0.827	0.713
	60°	92.55	0.734	0.598
	90°	94.76	0.705	0.560
Dimensionless	1	83.74	0.932	0.832
gravitational acceleration	5	94.76	0.733	0.598
(reference acceleration = 9.8 m/s^2)	10	107.98	0.58	0.337

state increases and the performance of a heat pipe deteriorates (because variation in R^* between the hot end to the cold end is greater). This is explained by the fact that a part of the capillary pumping overcomes the gravity and the heat pipe needs a lesser amount of coolant liquid because the initial radius of curvature is smaller.

The effect of variations in the thermophysical properties on the transient behavior of a micro heat pipe is summarized in Table 3. The radius of curvature with time monotonically decreases with time for each case and the initial and the steady-state values for dimensionless radius of curvature $X^* = 0.5$ are given in Table 3. With an increase in surface tension, the time to reach steady state decreases and the performance factor increases. This is explained by the fact that an increase in surface tension increases the capillary pumping available for flow. With an increase in viscosity, the time to reach steady state increases and the performance factor decreases because an increase in viscosity increases the friction loss. With an increase in contact angle, the time to reach steady state decreases and the performance factor increases, given that an increase in contact angle increases the accumulation of liquid in the groove for heat transfer.

The effect of the design parameters on the transient behavior is summarized in Table 4. The radius of curvature monotonically decreases with time for each case and the initial and the steady-state values for dimensionless radius of curvature $X^* = 0.5$ are given in Table 4. With an increase in length of heat pipe, the time to reach steady state increases and the performance factor decreases, given that an increase in the length of heat pipe increases the frictional loss. With an increase in friction factor, the time to reach steady state increases and the performance factor decreases, which is explained by the fact that an increase in friction factor increases the frictional loss. With an increase in the length of the adiabatic section, the time to reach steady state increases because an increase in the length of the adiabatic section increases the frictional loss. The variation in the performance factor cannot be obtained for the variation in the adiabatic length because the performance factor formula does not have its variation. However, the performance of a heat pipe diminishes as we increase the length of the adiabatic section[13] and here also we see that the variation in R^* increases with an increase in the length of the adiabatic section. With an increase in the fraction of the ungrooved area, the time to reach steady state increases and the performance factor decreases; that is, the larger the ungrooved area, the higher the velocity and thus the higher the frictional loss.

The simulations have been also tested by giving sinusoidal time-varying perturbation in viscosity, surface tension, and friction factor. The disturbances have been obtained in the transient profiles, but it was not decaying or growing with time; rather, it was steady with time. The effect of the disturbances was similar to the effect discussed with steady variations in previous paragraphs, such as if we increase the surface tension, the performance improves, and the opposite is true for the viscosity.

We now discuss how the presented model can handle some general issues in a micro heat pipe operation. First, we will discuss the difference in the mechanisms of evaporation and condensation. In this model, a detailed model for condensation or evaporation has not been presented; rather, an equation has been used to relate the evaporative and the condensing heat transfers to the fluid, heat, and mass transfer of the coolant fluid. The general nature of the model is capable of handing any functionality of the heat interaction in the condenser or the evaporator. Depending on the nature of the condensation or the evaporation, the functional variation of Q can be changed and the same model for the fluid, heat, and mass transfer of the coolant liquid can be used for this purpose. Second, is the difference in the contact angle between the evaporative and the condensing sections. The contact angle is an input parameter in the model and any functional variation can be fed into the model.

It is worth noting that the contact angle has a significant

Table 3. Effect of Variations in the Thermophysical Properties of Coolant Liquid on the Transient Behavior of a Micro Heat Pipe

Thermophysical Property	Deviation Value	t^* to Reach Steady State	R^* at $X^* = 0.5$ at $t^* = 0$	R^* at $X^* = 0.5$ at $t^* = 110.2$	Performance Factor
Surface tension	−5%	92.55	0.929	0.823	3.740
	0%	83.74	0.932	0.832	3.937
	5%	77.13	0.935	0.841	4.134
Viscosity	−5%	74.92	0.932	0.838	4.145
	0%	83.74	0.932	0.832	3.937
	5%	90.35	0.932	0.827	3.750
Contact angle	0°	83.74	0.932	0.832	3.939
	1°	79.33	0.931	0.855	4.994
	3°	68.31	0.930	0.880	7.450

Table 4. Effect of Design Parameters on the Transient Behavior of a Micro Heat Pipe

Parameter	Deviation/Dimensionless Value	t^* to Reach Steady State	R^* at $X^* = 0.5$ at $t^* = 0$	R^* at $X^* = 0.5$ at $t^* = 110.2$	Performance Factor
Dimensionless length	1	83.74	0.932	0.832	3.939
	1.5	94.76	0.901	0.734	2.625
	2.5	105.77	0.846	0.396	1.575
Friction factor	−5%	77.13	0.932	0.838	4.145
	0%	83.74	0.932	0.832	3.939
	5%	88.14	0.932	0.827	3.750
Fraction of length as adiabatic length	0.33	83.74	0.932	0.832	3.939**
	0.4	88.14	0.932	0.826	3.939**
	0.5	96.96	0.932	0.820	3.939**
Value of f_a for ungrooved area	0.00%	83.74	0.932	0.832	3.939
	0.05%	85.94	0.932	0.826	3.937
	0.08%	92.55	0.932	0.821	3.813

**Fraction of adiabatic length is not in performance factor formula.

effect on the performance of a micro heat pipe because of two reasons: (1) With an increase in the contact angle, the liquid accommodation capacity of the heat pipe increases. The more the amount of the coolant liquid available, without flooding the heat pipe, the more heat can be transfer using evaporation. (2) With an increase in the contact angle, the meniscus area increases and so more heat can be transferred for the same amount of heat flux. However, the important disadvantage that we have is that with an increase in the contact angle, the meniscus radius increases and so we have less capillary force available to pump the fluid.

Next, we discuss the effect of the vapor flow in a heat pipe. The flow of vapor in a heat pipe is as important as the fluid flow, given that for an operation of a heat pipe, the coolant liquid has to move from the cold end to the hot end and, in the same way, the vapor has to flow from the hot end to the cold end to have a continuous operation. First, if the vapor velocity is higher than the sonic limit, the heat pipe stops working. In this work it has been checked and it was found that the vapor velocity is much less than the sonic limit. The effect of the vapor flow at the liquid–vapor interface exerts shear stress at the liquid and it has also been considered in this work and it was found that the effect is negligible. The reason behind this phenomenon is that the vapor flow area is large and for the amount of heat input used in this work, the vapor velocity does not have a strong effect.

Conclusion

In the present study, we discuss fill charge, temperature, height, and thermal resistance of the coolant liquid, and the effect of the variations in the thermophysical properties and the design parameters in the transient operation of a V-shaped micro heat pipe. They have been calculated by use of a macroscopic approach. The study suggests that the fill charge is an important parameter for the efficient operation of a micro heat pipe. Both under- and overcharging deteriorate the performance of a micro heat pipe. The effect of overcharging is worse than that of undercharging. The coolant liquid height decreases with time. The difference in the liquid and the substrate temperatures was found to be significant. The effect of coolant liquid thermal conductivity is negligible in the axial heat transport. Higher the performance factor, the less time is required to reach the steady state.

Application of the present study is discussed here. First, it is useful for the start-up and shutdown of a micro heat pipe. Second, it gives the detailed analysis of the fill charge, which is a useful quantity for a heat pipe operation and also presents the effect of the over- and undercharges, which is helpful in the operation of a heat pipe. Third, it gives the liquid temperature and the liquid height, which are useful to understand the operation of a heat pipe. Fourth, the analysis presents the sensitivity analysis by varying the design and the thermophysical properties of the coolant liquid, which will guide the design of such system. Although the present report is a step forward in heat pipe research, for more realistic models, we should eliminate the assumption of predefined heat interaction between the liquid temperature and the solid substrate, and consider two-dimensional analysis of the system.

Acknowledgments

Correspondence and discussions with Professor Sunando DasGupta and Professor Sirshendu De and their valuable suggestions are gratefully acknowledged. The author would like to thank Prabhat Kumar for his help in sensitivity analysis calculations.

Notation

a = side length of a groove, m
A_{cs} = area of cross section of substrate, m^2
A_g = total vapor cross-sectional area, m^2
A_l = total liquid cross-sectional area, m^2
A_1 = liquid cross-sectional area with sharp corner, m^2
B_1 = constant in expression for A_l
B_2 = constant
Cp = specific heat capacity, J kg^{-1} $°C^{-1}$
D_h = hydraulic diameter, m
f = friction factor
f_a = fraction of the ungrooved area
f_o = flooded portion of condenser section
f_u = nondimensional radius of curvature at the cold end during under charge
g = acceleration arising from gravity, m/s^2
h = liquid height, m
K' = constant in expression for B_2
K_s = thermal conductivity of substrate, W m^{-1} K^{-1}
K_l = thermal conductivity of liquid, W m^{-1} K^{-1}

L = length of heat pipe, m
L_d = dry-out length of heat pipe, m
L_f = length of the flooded region in heat pipe, m
L_h = half of total wetted length, m
L_h = half of wetted length for one corner, m
m_f = fill charge, kg
N_{Re} = Reynolds number
P = pressure, N/m^2
P_{v_o} = pressure in vapor region, N/m^2
Q = net heat flux supplied to the liquid, W/m^2
Q_{avg} = average heat flux through the coolant liquid, W/m^2
Q_l = heat flux at substrate and liquid interface supplied to the liquid, W/m^2
Q_v = heat flux for vaporization of liquid, W/m^2
R = radius of curvature, m
R_m = meniscus surface area per unit length, m
R_{th} = thermal resistance, K m^{-2} W^{-1}
t = time, s
T = temperature, °C
T_{con} = temperature at the end of the condenser region, °C
V = axial velocity, m/s
w_b = polygon pitch, m
x = coordinate along the heat pipe, m
X^* = nondimensional coordinate along heat pipe
X_d^* = nondimensional coordinate of the onset of dry-out

Greek letters

α = half-apex angle of polygon, rad
β = inclination of substrate with horizontal, rad
γ = contact angle, rad
ϕ = curvature, m^{-1}
λ_l = latent heat of vaporization of coolant liquid, J/kg
μ_l = viscosity of coolant liquid, kg m^{-1} s^{-1}
ρ_l = density, kg/m^3
σ_l = surface tension of coolant liquid, N/m
τ = time constant, s^{-1}
τ_w = wall shear stress, N/m^2

Superscript

* = dimensionless

Subscripts

a = adiabatic
c = condenser
d = dry-out
e = evaporator
g = vapor
l = coolant liquid
o = reference
R = reference
s = substrate

Literature Cited

1. Cotter TP. Principles and prospects of micro heat pipes. Proceedings of the 5th International Heat Pipe Conference, Tsukuba, Japan; 1984:328-332.
2. Suman B, Hoda N. Effect of variations in thermophysical properties and design parameters on the performance of a V-shaped micro grooved heat pipe. *Int J Heat Mass Transfer.* 2005;48:2090-2101.
3. Swanson LW, Herdt GC. Model of the evaporative meniscus in a capillary tube. *J Heat Transfer.* 1992;114:434-441.
4. Mallik AK, Peterson GP, Weichold MH. On the use of micro heat pipes as an integral part of semiconductor devices. *J Electron Packaging.* 1992;114:436-442.
5. Mallik AK, Peterson GP. Transient response characteristics of vapor deposited micro heat pipe. *J Electron Packaging.* 1995;117:82-87.
6. Peterson GP, Duncan AB, Weichold MH. Experimental investigation of micro heat pipes fabricated in silicon wafers. *J Heat Transfer.* 1993;115:750-756.
7. Babin BR, Peterson GP, Wu D. Steady state modeling and testing of a micro heat pipe. *J Heat Transfer.* 1990;112: 595-601.
8. Wu D, Peterson GP. Investigation of the transient characteristics of a micro heat pipe. *J Thermophys Heat Transfer.* 1991;5:129-134.
9. Khrustalev D, Faghri A. Thermal analysis of a micro heat pipe. *J Heat Transfer.* 1994;116:189-198.
10. Xu X, Carey VP. Film evaporation from a micro-grooved surface—An approximate heat transfer model and its comparison with experimental data. *J Thermophys Heat Transfer.* 1990;4:512-520.
11. Catton I, Stores GR, A semi-analytical model to predict the capillary limit of heated inclined triangular capillary grooves. *J Heat Transfer.* 2002;124:162-168.
12. Suman B, De S, DasGupta S. A model of the capillary limit of a micro grooved heat pipe and the prediction of dry out length. *Int J Heat Fluid Flow.* 2005;26:495-505.
13. Suman B, Kumar P. An analytical model for fluid flow and heat transfer in a micro heat pipe of polygonal shape. *Int J Heat Mass Transfer.* 2005;48:4498-4509.
14. Tio KK, Liu CY, Toh KC. Thermal analysis of micro heat pipes using a porous medium model. *Heat Mass Transfer.* 2000;36:21-28.
15. Ochterbeck JM. Heat pipes. In Bejan A, Kraus AD, eds. *Heat Transfer Handbook*. Hoboken, NJ: Wiley; 2003.
16. Duncan AB, Peterson GP. Charge optimization for triangular shaped etched micro heat pipe. *AIAA J Thermophys Heat Transfer.* 1995;9:365-367.
17. Wayner PC Jr. The effect of interfacial mass transport on flow in thin liquid films. *Colloids Surf.* 1991;52:71-84.
18. Wu D, Peterson GP, Chang WS. Transient experimental investigation of micro heat pipes. *J Thermophys Heat Transfer.* 1991;5:129-134.
19. Chang WS, Colwell GT. Mathematical modeling of the transient operation characteristics of a low temperature heat pipe. *Numer Heat Transfer.* 1985;8:169-186.
20. Faghri A, Chen MM. A numerical analysis of the effects of conjugate heat transfer, vapor compressibility, and viscous dissipation in heat pipe. *Numer Heat Transfer A.* 1989;16:389-405.
21. Turnier JM, El-Genk MS. A heat pipe transient analysis model. *Int J Heat Mass Transfer.* 1994;37:753-762.
22. Zhu N, Vafai K. Analytical modeling of startup characteristics of asymmetric flat-plate and disc-shaped heat pipes. *Int J Heat Mass Transfer.* 1998;41:2619-2637.
23. Doster JM, Hall ML. Numerical modeling of high-temperature liquid metal heat pipes. 89-HT-13 1-9. Proceedings of the 1989 Joint ASME/AIChE National Heat Transfer Conference, Philadelphia, PA; 1989.
24. Colwell GT, Chang WS. Measurement of transient behavior of a capillary structure under the heavy thermal loading. *Int J Heat Mass Transfer.* 1984;27:541-551.
25. Chang WS. *Heat Pipe Start Up from the Supercritical State*. PhD Dissertation. Atlanta, GA: School of Mechanical Engineering, Georgia Institute of Technology; 1981.
26. Wang Y, Vafai K. An experimental investigation of the transient characteristics on a flat-plate heat pipe during startup and shutdown operations. *J Heat Transfer.* 2000;122:525-535.
27. Suman B, De S, DasGupta S. Transient modeling of micro groove heat pipe. *Int J Heat Mass Transfer.* 2005;48:1633-1646.
28. Suman B, Hoda N. On the transient analysis of a V-shaped micro heat pipe. *J Heat Transfer.* 2006, submitted.
29. Ravikumar M, DasGupta, S. Modeling of evaporation from V-shaped microgrooves. *Chem Eng Commun.* 1997;160:225-248.
30. Peterson GP, Ma HB. Theoretical analysis of the maximum heat transport in triangular grooves: A study of idealized micro heat pipe. *J Heat Transfer.* 1996;118:731-739.
31. Ha JM, Peterson GP. Analytical prediction of axial dry-out point for evaporating liquids in axial microgrooves. *J Heat Transfer.* 1998;120:452-457.
32. Keblinski P, Phillpot SR, Choi USU, Eastman JA. Mechanism of heat flow in suspensions of nano-sized particles (nanofluids). *Int J Heat Mass Transfer.* 2002;45:855-863.

Appendix

$$R_o = \frac{a \sin \alpha}{\cos(\alpha + \gamma)}$$

where a is the side length of V-shaped groove.

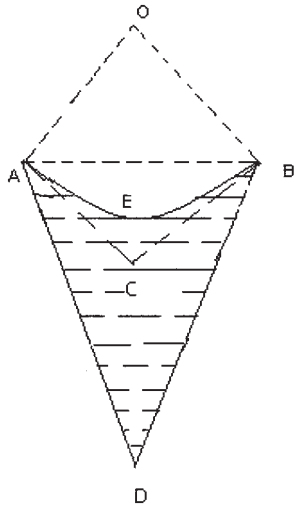

Figure A1. Geometry of V-shaped heat pipe.

$$w_b = 2a$$

The geometry of a V-shaped heat pipe is presented in Figure A1 (refer to Figure 1).

The shaded area in Figure A1is the cross-sectional area of the liquid in the heat pipe when the ungrooved radius is zero. The cross-sectional area of one corner is expressed as A_l = Area of $ABCD$ + Area of ΔABC − (Area of sector AOB − Area of ΔAOB).

The line diagram of section OBD in Figure A1 is presented in Figure A2 in detail.

From Figure A1, AC and BC are the tangents to the liquid meniscus.

$$\angle CAD = \gamma$$

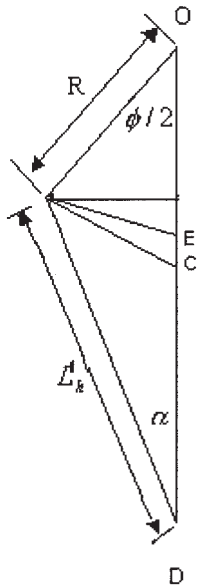

Figure A2. Line diagram of section *OBD* in Figure A1.

$$\angle ADC = \alpha$$

$$\angle ACB = 2(\alpha + \gamma)$$

$$\angle AOB = \phi = \pi - 2(\alpha + \gamma)$$

$$R_o = \frac{a \sin \alpha}{2 \cos(\alpha + \gamma)}$$

$$L'_h = R \frac{\cos(\alpha + \gamma)}{\tan \alpha}$$

$$L_h = nL'_h$$

$$R_m = R\phi$$

Here $n = 2$ because we consider a V-groove.

The liquid height, h, is DE, which can be calculated as follows:

$$h = OD - OE = L'_h \cos \alpha + R \cos \frac{\phi}{2} - R$$

$$= R\left[\frac{\cos(\alpha + \gamma)}{\tan \alpha} + \sin(\alpha + \gamma) - 1\right]$$

$$\text{Area of } ACBD = \frac{R^2 \cot(\alpha + \gamma)\cos(\alpha + \gamma)\sin \gamma}{\sin \alpha}$$

$$\text{Area of } \Delta ABC = R^2 \cot(\alpha + \gamma)\cos^2(\alpha + \gamma)$$

$$\text{Area of sector } AOB = \phi R^2/2$$

$$\text{Area of } \Delta AOB = R^2 \cos(\alpha + \gamma)\sin(\alpha + \gamma)$$

Thus

$$A'_l = R^2\left[\{\cot(\alpha + \gamma) - \Phi/2\} + \frac{\cot(\alpha + \gamma)\cos(\alpha + \gamma)\sin \gamma}{\sin \alpha}\right]$$

$$= B_1 R^2$$

$$A_l = B_1(R^2 - f_a R_o^2)$$

where

$$B_1 = \left[\{\cot(\alpha + \gamma) - \Phi/2\} + \frac{\cot(\alpha + \gamma)\cos(\alpha + \gamma)\sin \gamma}{\sin \alpha}\right]$$

f_a = Square of the fraction of ungrooved radius

= fraction of the ungrooved area

$$B_2 = \frac{\mu_l K' \cos^2(\alpha + \gamma)}{2 \sin^2 \alpha\left[\frac{\cot(\alpha + \gamma)\cos(\alpha + \gamma)\sin \gamma}{\sin \alpha} + \{\cot(\alpha + \gamma) - \Phi/2\}\right]^2}$$

Manuscript received Nov. 28, 2005, revision received Apr. 19, 2006, and final revision received Jun. 5, 2006.